

# Single-Molecule Imaging of Lateral Mobility and Ion Channel Activity in Lipid Bilayers using Total Internal Reflection Fluorescence (TIRF) Microscopy

Shuo Wang<sup>1</sup>, Stephan Nussberger<sup>1</sup>

<sup>1</sup> Biophysics Department, Institute of Biomaterials and Biomolecular Systems, University of Stuttgart

## Corresponding Author

Stephan Nussberger

stephan.nussberger@bio.uni-stuttgart.de

## Citation

Wang, S., Nussberger, S. Single-Molecule Imaging of Lateral Mobility and Ion Channel Activity in Lipid Bilayers using Total Internal Reflection Fluorescence (TIRF) Microscopy. *J. Vis. Exp.* (192), e64970, doi:10.3791/64970 (2023).

## Date Published

February 17, 2023

## DOI

10.3791/64970

## URL

jove.com/video/64970

## Abstract

High-resolution imaging techniques have shown that many ion channels are not static, but subject to highly dynamic processes, including the transient association of pore-forming and auxiliary subunits, lateral diffusion, and clustering with other proteins. However, the relationship between lateral diffusion and function is poorly understood. To approach this problem, we describe how lateral mobility and activity of individual channels in supported lipid membranes can be monitored and correlated using total internal reflection fluorescence (TIRF) microscopy. Membranes are fabricated on an ultrathin hydrogel substrate using the droplet interface bilayer (DIB) technique. Compared to other types of model membranes, these membranes have the advantage of being mechanically robust and suitable for highly sensitive analytical techniques. This protocol measures  $\text{Ca}^{2+}$  ion flux through single channels by observing the fluorescence emission of a  $\text{Ca}^{2+}$ -sensitive dye in close proximity to the membrane. In contrast to classical single-molecule tracking approaches, no fluorescent fusion proteins or labels, which can interfere with lateral movement and function in the membrane, are required. Possible changes in ion flux associated with conformational changes of the protein are only due to protein lateral motion in the membrane. Representative results are shown using the mitochondrial protein translocation channel TOM-CC and the bacterial channel OmpF. In contrast to OmpF, the gating of TOM-CC is very sensitive to molecular confinement and the nature of lateral diffusion. Hence, supported droplet-interface bilayers are a powerful tool to characterize the link between lateral diffusion and the function of ion channels.

## Introduction

The present protocol aims to describe how to study the correlation between membrane mobility and ion channel

permeability of membrane proteins in polymer-supported droplet-interface bilayer (DIB) membranes<sup>1,2,3</sup>.

The present technique complements an impressive array of advanced optical and surface analytical tools, such as single particle tracking<sup>4,5</sup>, fluorescence correlation spectroscopy<sup>6,7</sup>, and high-speed atomic force microscopy<sup>8,9,10</sup>. These provide valuable insights into the dynamic composition and structure of membranes that influence membrane-based reactions<sup>11,12,13</sup>. While the movement and lateral diffusion of proteins depends on the local density of proteins in the membrane, individual protein molecules can also be trapped in lipid rafts<sup>14</sup> and by protein-protein interactions<sup>15,16</sup>. Depending on the protein domains protruding from the membrane into the extracellular environment or cytosol, protein mobility can vary from highly mobile to completely immobile. However, due to the complexity of the membrane and its peripheral structures, it is often difficult to decipher the interplay between the nature of lateral mobility and protein function<sup>17</sup>.

DIB membranes have proven to be an efficient platform for biophysical single-molecule analyses of membrane proteins<sup>18,19,20,21,22</sup>. They are formed by lipid self-assembly through the contact of aqueous droplets with hydrogel-supported substrates in a lipid/oil phase. Similar to the commonly used supported lipid bilayers (SLBs)<sup>1,23,24,25</sup>, DIBs allow local tuning of the lateral mobility by temporary or permanent binding of proteins to the polymer matrix when functionalized with suitable ligands<sup>17</sup>. The latter can serve as a model system for biochemical processes in cell membranes with a heterogeneous protein distribution<sup>10</sup>.

The experimental approach described here relies on the fluorescence of Ca<sup>2+</sup>-sensitive dyes to measure the Ca<sup>2+</sup>

ion flux through individual channels in close proximity to the membrane<sup>2,22</sup> using TIRF microscopy. This optical approach limits the illumination of the sample to a distance close to the membrane, which, due to the physical properties of the evanescent excitation light, leads to a significant reduction of the fluorescence background. The latter is a prerequisite if high spatial and temporal resolution is required for the detection of single molecules. In contrast to classical electrophysiological methods<sup>26,27</sup>, no membrane voltages are required to study ion flux through individual channels. Furthermore, the method does not require labeling with fluorescent dyes or molecules that could interfere with the lateral movement of the channels in the membrane.

The method is particularly useful for studying protein channels embedded in the membrane at the single molecule level without using classical electrophysiology. Using mitochondrial protein-conducting channel TOM-CC from *Neurospora crassa*<sup>28,29,30</sup> and OmpF, which supports the diffusion of small hydrophilic molecules across the outer membrane of *Escherichia coli*<sup>17,31</sup>, we illustrate how the membrane mobilities and channel activities of the two proteins can be studied and correlated. We suggest that this approach, although optimized for TOM-CC and OmpF, can be readily applied to other protein channels.

## Protocol

### 1. Protein production

**NOTE:** This section describes the procedure for isolating OmpF from *Escherichia coli* BE BL21(DE3) omp6<sup>31,32</sup>, which lacks LamB and OmpC, and TOM core complex from *Neurospora crassa* (**Figure 1**)<sup>28,29</sup>. The latter requires mitochondria isolated from a *N. crassa* strain<sup>28</sup> containing a 6xHis-labeled form of the TOM subunit Tom22 (**Figure 1A**),

which can be isolated as described<sup>28</sup>. The following protocols usually yield 1-2 mg of *N. crassa* TOM-CC and 10 mg of *E. coli* OmpF. If the amount is to be adjusted, it is important that the protein/detergent ratios are precisely maintained. Unless otherwise specified, all steps should be performed at 4 °C.

#### 1. Isolation of TOM core complex

1. Solubilize purified *N. crassa* mitochondria (2 g of protein) obtained by differential sedimentation from approximately 1.5 kg (wet weight) hyphae, according to Bausewein et al.<sup>30</sup>, at a protein concentration of 10 mg/mL in 20 mM Tris-HCl (pH 8.5), 1% (w/v) DDM, 20% (v/v) glycerol, 300 mM NaCl, 20 mM imidazole, and 1 mM phenylmethylsulfonyl fluoride (PMSF) for 30 min at 4 °C.

**CAUTION:** PMSF is toxic. Wear appropriate personal protective equipment.

2. Transfer the solubilized mitochondria into ultracentrifuge tubes and separate the non-solubilized membranes from solubilized membrane proteins by ultracentrifugation at 130,000 x *g* for 40 min at 4 °C and filtration with standard-grade filter paper.
3. Equilibrate a prepacked Ni-NTA column (volume of 5 mL) with about 5 column volumes (CV) of buffer A1 (**Table 1**) using an automated protein purification system. Run the Ni-NTA column at a constant flow rate of 1 mL/min during all steps. Use a lower volume column (1 mL) if the proteins have been isolated from less than 2 g of mitochondria.
4. Load the solubilized protein sample onto the Ni-NTA column at a flow rate of 1 mL/min.

5. Wash the Ni-NTA column with 5 CV of buffer A1 (**Table 1**) to remove unbound proteins.
6. Elute His-tagged TOM-CC with 30% buffer A2 (**Table 1**; 300 mM imidazole) and collect the protein peak as it appears in the 280 nm chromatogram (**Figure 1B**).
7. For further purification of TOM-CC, equilibrate the prepacked anion exchange column (1 mL) with 5 CV each of buffer B1, B2, and B1 (**Table 1**) using the automated protein purification system. Run the anion exchange column at a constant flow rate of 1 mL/min during all steps.
8. Load the TOM-CC peak fraction (step 1.1.6) on the anion exchange column (flow rate of 1 mL/min).
9. Remove the unbound proteins by washing the column with 5 CV of buffer B1 (**Table 1**) and a linear salt gradient of 0%-20% buffer B2 (**Table 1**).
10. Elute TOM-CC with a linear salt gradient of 20%-35% buffer B2, and collect the protein peak fraction as it appears in the 280 nm chromatogram (**Figure 1C**).
11. Assess the sample purity by SDS-PAGE (**Figure 1D**) and determine the protein concentration using a commercially available protein assay, according to the manufacturer's protocol (see **Table of Materials**).
12. Freeze the protein samples in liquid nitrogen and store them at -80 °C until further use.

**CAUTION:** Liquid nitrogen should be handled in well-ventilated areas. Wear appropriate personal protective equipment.

## 2. Isolation of OmpF

1. Recover the *E. coli* strain BE BL21(DE3) omp6, lacking LamB and OmpC<sup>32</sup>, from a frozen glycerol stock under sterile conditions, and streak onto a Luria-Bertani (LB) agar plate (**Table 2**). To do this, gradually spread the sample evenly over the entire plate.
2. Allow the sample to soak into the agar for 5 min, before inverting the plate with the lid closed and incubating overnight at 37 °C.
3. Select a single *E. coli* colony, inoculate 7.5 mL of LB medium (**Table 2**) with this single colony using a sterile toothpick, and leave to grow overnight (14 h) with agitation (170 rpm) at 37 °C.
4. Transfer 2 x 1 mL of *E. coli* cells with sterile pipettes into 2 x 500 mL of LB medium (**Table 2**), and leave to grow overnight (~14 h) at 37 °C with agitation (~170 rpm) in a shaker.
5. Harvest the cells by centrifugation at 5,000 x g for 20 min at 4 °C, freeze the pellet in liquid nitrogen, and store at -80 °C until further use.

**NOTE:** The wet weight of the cell pellet is typically 5 g per 1 L of culture. At this point, the protocol can be paused.

6. Thaw and resuspend the cells (2 g) in 20 mL of lysis buffer C1 (**Table 2**), and pass the suspension three times at 1,000 psi through a precooled (4 °C) high-pressure cell disruption system, with a maximum sample volume of 35 mL, according to the manufacturer's instructions.

**CAUTION:** The use of a French press can lead to serious injuries. Never exceed the pressure limit of

the cell used. Wear appropriate personal protective equipment.

7. Remove unbroken cells from the lysate by centrifugation at 4,000 x g for 15 min, and collect the supernatant.
8. Collect the membranes by ultracentrifugation at 100,000 x g for 1 h.
9. Resuspend the membrane pellet in 10 mL of buffer C2 (**Table 2**), and mix with an equal volume of SDS buffer C3 (**Table 2**) using a ball-bearing glass homogenizer.
 

**CAUTION:** β-mercaptoethanol in buffer C3 is toxic. Follow all relevant safety regulations.
10. Incubate the suspension in a water bath at 50 °C for 30 min.
11. Centrifuge the sample at 100,000 x g at 20 °C for 1 h.
12. Resuspend the membrane pellet in 10 mL of SDS buffer C4 (**Table 2**) using a ball-bearing glass homogenizer, and incubate the suspension in a water bath at 37 °C for 30 min.
 

**NOTE:** If the pellet cannot be resuspended, add more SDS buffer C4 up to a volume of 20 mL.
13. Centrifuge the sample at 100,000 x g at 20 °C for 30 min, and collect the supernatant.
14. Mix the supernatant with octyl polyoxyethylene (octyl POE) to a final detergent concentration of 0.5% (w/v), and dialyze the sample twice against buffer C5 (**Table 2**) at 4 °C for 24 h. For this purpose, use dialysis tubing with a cut off of 20 kDa, according to the manufacturer's instructions, and place the sample in the dialysis tubing or device.

**NOTE:** The cut off of the dialysis tubing needs to be adjusted should proteins with other molecular masses be dialyzed.

15. Assess the sample purity by SDS-PAGE and determine the protein concentration using a commercially available protein assay, according to the manufacturer's protocol (**Table of Materials**).

**NOTE:** Samples heated to 95 °C show monomeric OmpF. Samples not heated show OmpF in its trimeric form (**Figure 1F**).

16. Shock-freeze dialyzed OmpF in aliquots in liquid nitrogen, and store at -20 °C until further use.

**CAUTION:** Liquid nitrogen should be handled in well-ventilated areas. Wear appropriate personal protective equipment.

## 2. Optical single-channel recording of ion channels in DIB membranes

**NOTE:** This section describes the procedure for preparing DIB membranes in microfabricated polymethyl methacrylate (PMMA) chambers<sup>2</sup> to monitor lateral protein movement and ion flux through single ion channels<sup>17</sup>. The dimensions and exact drawings for manufacturing the chamber can be found in Lepthin et al.<sup>2</sup>. **Figure 2** gives an overview of the assembly of the PMMA chamber<sup>2</sup> and the formation of the DIB membranes. Unless otherwise specified, all steps are performed at room temperature (RT). **Figure 3** shows a schematic representation of a DIB membrane and how Ca<sup>2+</sup> flux through a single channel protein is used to monitor both movement in the membrane and the open-closed state of the channel.

1. Preparation of lipids

1. Remove the lipid stock solution containing 1,2-diphytanoyl-*sn*-glycero-3-phosphocholine (25 mg/mL DPhPC) dissolved in chloroform from the freezer at -20 °C, and warm to RT. For this purpose, it is generally sufficient to warm up the sample slowly by hand for a few minutes.

**CAUTION:** Chloroform is toxic. Wear appropriate personal protective equipment and perform all procedures involving chloroform under a fume hood.

2. Transfer 380 µL of DPhPC stock solution (25 mg/mL DPhPC) into a glass vial. Avoid pipettes with rubber sealings. Instead, use microliter glass syringes with stainless steel plungers.
  3. After handling the lipid stock solution, overlay the lipid stock solution with Ar or N<sub>2</sub> gas to prevent lipid oxidation. Use the lowest possible gas flow to avoid evaporation of the organic solvent in which the lipids are dissolved or splashing of the solvent sprays from the vial. Make sure that the lids of the glass vials containing lipids with organic solvent are coated with polytetrafluoroethylene (PTFE) on the inside.
  4. Dry the lipid sample (step 2.1.2) under a stream of N<sub>2</sub>, and remove the remaining organic solvent from the lipid sample overnight under vacuum (2.0 mbar) using an oil-free vacuum pump.
  5. Dissolve the lipid film in hexadecane/silicone oil solution by adding equal volumes of hexadecane and silicone oil (500 µL each) using a microliter glass syringe to a final lipid concentration of 9.5 mg/mL.
- NOTE:** The lipid solution is stable at RT for several weeks.

2. Preparation of agarose hydrogel

1. Prepare approximately 1 mL of low melting agarose solution (0.75% [w/v]) in double deionized water, and heat to 85 °C in a heating block for 20 min to be used for spin coating glass coverslips.
 

**NOTE:** The agarose solution can be kept at RT for several weeks and can be reheated several times.
2. Prepare low melting 2.5% (w/v) agarose solution in 0.66 M CaCl<sub>2</sub> and 8.8 mM HEPES (pH 7.2), and heat to 85 °C in a heating block for 20 min. Make sure that the agarose is well melted.
 

**NOTE:** The agarose solution can be kept for several weeks at RT and can be reheated several times, just like the agarose (step 2.2.1) used for spin coating.
3. Polymethyl methacrylate (PMMA) chamber assembly and lipid monolayer formation at the hydrogel hexadecane/silicone oil interface
  1. Place some glass coverslips (40 mm x 24 mm x 0.13 mm) into a stainless-steel coverslip holder, and clean them in a glass beaker for 10 min with acetone in an ultrasonic cleaner. Use just enough acetone to submerge the coverslips and cover the beaker loosely with a glass plate to create a pressureless, closed system that minimizes the escape of vapors during the cleaning process.
 

**CAUTION:** Acetone is a highly flammable solvent with a low flash point. Vapor/air mixtures are explosive. Operate the ultrasonic cleaner in a well-ventilated area. Wear appropriate personal protective equipment and observe official safety precautions (e.g., no open flames and no sparks).
  2. Rinse the glass coverslips with double-deionized water and dry them under a stream of N<sub>2</sub>.
- NOTE:** Coverslips cleaned in this way can be stored for several weeks.
3. Further clean and hydrophilize a coverslip in a plasma cleaner with oxygen (0.5 mbar) for 5 min.
 

**NOTE:** Carry out this step immediately before spin coating with agarose solution, as the hydrophilic effect of plasma cleaning wears off over time.
4. Mount a plasma-treated coverslip on a spin coater (**Figure 2**, step 1).
5. Coat the coverslip with a submicrometer-thick film of agarose by slowly adding 140 µL of heated 0.75% (w/v) low-melting agarose (step 2.2.1) at 3,000 rpm for 30 s, using a 200 µL pipette (**Figure 2**, step 1).
 

**NOTE:** The thickness of the agarose film can be determined by atomic force microscopy (AFM), as described<sup>17</sup>.
6. Immediately attach the spin-coated coverslip with the thin layer of the agarose hydrogel to the underside of the PMMA chamber<sup>2</sup>. Ensure that the agarose hydrogel points upward (**Figure 2**, step 2).
7. Fix the edges of the coverslip to the PMMA micro-machined device with transparent adhesive tape.
8. Place the PMMA device on a hot plate heated to 35 °C (**Figure 2**, step 3).
9. Carefully pour 200 µL of 2.5% agarose solution (step 2.2.2) into the inlet of the chamber with a pipette (**Figure 2**, step 3), without creating air bubbles so that the thin hydrogel applied by spin coating can equilibrate with the buffer of the 2.5% agarose solution and remain hydrated. Ensure that the 2.5% agarose solution is spread around the spin-coated agarose hydrogel but not over it (**Figure 3A**),

which can be avoided by gently pressing the PMMA chamber onto the heating plate.

10. Immediately cover the wells of the PMMA chamber (**Figure 2**, step 4) with a total of 60  $\mu\text{L}$  of lipid/oil solution (step 2.1.5), to initiate lipid monolayer formation at the agarose-oil interface and to avoid dehydration of the spin-coated agarose in the wells of the PMMA chamber. Keep the device on a hot plate at 35  $^{\circ}\text{C}$  for about 2 h.

**NOTE:** The circular wells in the PMMA chamber have a diameter of 0.5 mm and a depth of 1.8 mm, according to previously published work<sup>2</sup>.

#### 4. Preparation of lipid-coated aqueous droplets in hexadecane/silicone oil solution

1. Place 20  $\mu\text{L}$  of lipid hexadecane/silicone oil solution (step 2.1.5) to each of several microfabricated wells in a droplet incubation chamber (**Figure 2**, step 4). Suitable containers for the lipid hexadecane/silicone oil solution are small recesses of 40 mm x 30 mm x 3.5 mm in a thin PMMA plate<sup>2</sup>.
2. Prepare a microcapillary glass needle with a tip opening diameter of 20  $\mu\text{m}$  using a vertical or horizontal micropipette puller (e.g., used for making patch pipettes or sharp glass electrodes). Estimate the opening diameter of the microcapillary glass needle under a binocular stereomicroscope at low magnification, in a zoom range between 7.5x and 35x.

**NOTE:** The settings for the preheating mode before the glass capillary is pulled, the heating mode for pulling, and the traction force should be determined experimentally in advance, according

to the manufacturer's specifications of the pulling device and the type of capillary.

3. Fill the microcapillary glass needle with 5  $\mu\text{L}$  of aqueous injection solution containing 8.8 mM HEPES (pH 7.2), 7  $\mu\text{M}$  Fluo-8, 400  $\mu\text{M}$  EDTA, 1.32 M KCl, and 30 nM TOM core complex, or alternatively 20 nM OmpF using a microcapillary pipette tip. Use only double-distilled water previously treated with a chelating resin that binds multivalent metal ions ( $\text{Ca}^{2+}$ ) to prepare the aqueous injection solution.
  4. Mount the microcapillary glass needle with the aqueous injection solution on a piezo-driven nanoinjector.
  5. Inject 100-200 nL of aqueous droplets (**Figure 2**, step 4) containing 8.8 mM HEPES (pH 7.2), 7  $\mu\text{M}$  Fluo-8, 400  $\mu\text{M}$  EDTA, 1.32 M KCl, and 30 nM TOM core complex (step 1.1.12), or alternatively 20 nM OmpF (step 1.2.16) into the wells in the droplet incubation chamber filled with lipid hexadecane/silicone oil solution (see 2.1.5) using the nanoinjector. Make sure that the droplets do not touch each other by placing them several millimeters (>10 mm) apart into the wells. Otherwise, if lipid monolayers have not yet formed at the oil/buffer interface, they will merge into larger droplets.
- NOTE:** If no glass capillaries and no nanoinjectors are available, the droplets can alternatively be prepared manually with single-channel microliter pipettes for volumes between 0.1  $\mu\text{L}$  and 0.5  $\mu\text{L}$ , as described<sup>2</sup>. In this case, however, the droplet volumes are not as accurate.
6. Allow the formation of a lipid monolayer at the droplet/oil interface for about 2 h by maintaining the

- PMMA and droplet incubation chambers (**Figure 2**, step 4) on a hot plate heated to 35 °C.
5. Preparation and imaging of single ion channels in DIB membranes
    1. Manually transfer individual aqueous droplets from the wells of the droplet incubation chamber under a stereomicroscope into the wells of the PMMA chamber (**Figure 2**, step 5), using a single-channel microliter pipette with a 10  $\mu$ L disposable polypropylene tip. Allow the droplets to sink onto the lipid monolayers formed at the hydrogel-oil interfaces for about 5 min to form a lipid bilayer (**Figure 3**) between the droplets and the agarose hydrogel.
    2. Mount the PMMA chamber with DIB membranes on the sample holder of an inverted light microscope and assess membrane formation using a 10x Hoffman modulation contrast objective (**Figure 2**, step 6). DIB membrane formation is indicated by a clear white ring at the interface between the droplet and the hydrogel (**Figure 4A**). DIB membranes that have been broken do not show this ring (**Figure 4B**).  
**NOTE:** Alternatively, the DIB membranes can be visualized at 10x magnification by phase contrast or differential interference contrast (DIC) microscopy.
    3. If DIB membranes have formed, mount the PMMA chamber on the sample holder of a TIRF microscope (**Figure 2**, step 7) equipped with a conventional light source for epifluorescence illumination, a 488 nm laser ( $P_{\text{max}} = 100$  mW), and a back-illuminated electron-multiplying CCD camera (512 x 512 pixels; >95% QE) to achieve a pixel size of  $\sim 0.16$   $\mu$ m.
      4. Focus the edge of a DIB membrane with a 10x magnification objective under epifluorescence illumination with a high-intensity light source using a GFP filter set.
      5. Fine focus the same edge of the DIB membrane at high magnification with a 100x/N.A. 1.49 apochromat oil TIRF objective, again under epifluorescence illumination, with the high-intensity light source using a GFP filter set that allows visualizing weak background fluorescence of the fluorescent dye Fluo-8 in the droplet (**Figure 4C**).
      6. Change the filter setting from GFP to the quad-band TIRF filter set.
      7. Switch on the 488 nm laser and set the intensity of the laser on the objective lens to a value between 8 mW and 10 mW.  
**NOTE:** Since there is often no quantitative information on the laser intensity at the objective lens, the laser intensity settings should be calibrated beforehand in separate measurements at the lens, with an optical laser power meter equipped with a photodiode sensor, according to the manufacturer's specifications.  
**CAUTION:** To ensure safe operation of the laser, the operator must be aware of the possible dangers of laser radiation and the accident prevention regulations.
      8. To visualize single ion channels, adjust the TIRF angle and EMCCD camera gain (e.g., EM gain multiplier setting: 285) so that open ion channels in the DIB membrane appear as high-contrast fluorescent spots on a dark background (**Figure 4D-G**), and the signal-to-background ratio, when

visually inspected, reaches a maximum. Ensure that the spots, corresponding to  $\text{Ca}^{2+}$ -flux through single ion channels, remain in focus and have a round shape, with high intensity in the center and gradually decreasing toward the periphery. Membranes without channels show only background fluorescence (**Figure 4C**).

9. Before recording the movement and open-closed activity of individual channels over time, check that fluorescent spots are in focus, to ensure that the ion channels have reconstituted into the DIB membranes and are moving laterally in the membrane plane. If this is not the case, it could indicate that a fluorescent molecule is dipping in and out of the evanescent field generated by the laser near the membrane.
10. Record a series of membrane images that allows proper tracking of the position and monitoring of the open-closed state of the individual ion channels. To determine the type of lateral mobility (e.g., free motion vs transient anchorage [for reference, see<sup>16</sup>]) and the state of channel activity (e.g., open or closed), acquire sufficiently long (e.g., 30 s to 1 min) and well-sampled trajectories (e.g., frame rate of  $48 \text{ s}^{-1}$ ).

**NOTE:** The observation of channeled, restricted, or hop diffusion<sup>16</sup> requires that the sampling rate is sufficiently fast to measure unrestricted diffusion within confining boundaries. In addition, ensure that the data sampling time is sufficiently long to measure the transition from unconstrained to constrained diffusion (for details, see Jacobson et al.<sup>16</sup>).

## 6. Image and data processing

**NOTE:** Open-source image processing packages<sup>33</sup> or self-written routines<sup>17</sup> based on commercial software packages can be used to analyze the spatiotemporal dynamics of individual ion channels in DIBs. To be able to correlate lateral membrane mobility with the ion flux through the individual channels, no filter algorithms should be applied.

1. Correct image time series for bleaching by applying standard procedures<sup>34</sup> using self-written routines, by fitting the average frame intensity  $\langle I(t)_{raw} \rangle$  of the full image to  $f(t, a_k) = a_1 \exp(a_2 t) + a_3 \exp(a_4 t)$ , where  $t$  is the frame index (time) and  $a_k$  is the fitting parameters. Then, correct the time series according to  $I(t) = I_{raw}(t) / f(t, a_k)$ , where  $I(t)$  is the intensity. Alternatively, for initial data analyses, perform background corrections by using open source software with implemented rolling-ball algorithms<sup>33</sup> and a rolling-ball radius, depending on the spot and pixel size of the camera (e.g., 50 pixels).
2. Determine the spatial positions and amplitudes of a fluorescence spot within a defined region of interest (ROI) (e.g., 30 x 30 pixels), by fitting  $I(t)$  at a given time  $t$  to a two-dimensional Gaussian function with planar tilt that accounts for possible local illumination gradients according to  $G_{2D}(x, \mu, p_k) = p_1 + p_{2,3}(x - \mu) + A \exp(-(x - \mu)^2 / 2\sigma^2)$ . Here,  $x = (x, y)$  is the ROI with the fluorescence intensity information,  $A$  and  $\sigma$  are the amplitude and widths of the Gaussian,  $p_k$  are parameters that characterize the background intensity of the ROI, and  $\mu = (x_0, y_0)$  defines the position of the Gaussian. The ion flux through an individual channel is given by the parameter  $A$ . The trajectory of the

channel is given by  $x$ , and allows for determining the lateral mobility of the channel. Alternatively, it is possible to determine the positions and intensities of individual spots using open-source platforms<sup>33</sup> and plug-ins as described<sup>35,36</sup>. Estimate the positional accuracy<sup>37</sup> after conversion of the EMCCD camera readout into photon numbers<sup>38</sup>.

3. Plot the fluorescence amplitude  $A$  versus time and the corresponding trajectory  $x$  to determine a possible correlation between the channel diffusivity and the ion flux through the channel. Perform this with any graphics software. In case of free lateral channel movement, determine the lateral diffusion coefficient  $D$  by linear regression of the time delay  $\tau$ , and calculate the mean square displacement of the spots from  $x$  according to  $D = \langle |r(x, y, \tau) - r(x_0, y_0, \tau)|^2 \rangle / 4\tau$ .

**NOTE:** Typical diffusion coefficients<sup>17</sup> for TOM-CC and OmpF freely moving in DIB membranes range between  $0.5$  and  $1.5 \mu\text{m}^2 \text{s}^{-1}$ . Molecules whose diffusion constant is less than  $0.01 \text{mm}^2 \cdot \text{s}^{-1}$  are defined as immobilized<sup>17</sup>.

## Representative Results

Real-time electrode-free optical single-channel recording reveals the interplay between lateral protein movement and

the function of individual ion channels in DIB membranes. Reconstitution of the mitochondrial TOM core complex (**Figure 1A**) into a DIB membrane (**Figure 4D**) illustrates a strong temporal correlation between lateral mobility and ion permeability (**Figure 5A**). The TOM-CC gating appears to be sensitive to the mode of lateral movement<sup>17</sup>. Moving channels show  $\text{Ca}^{2+}$  flux through their pores and high fluorescence point intensities. Trapped, non-moving molecules show low and medium fluorescence intensities. For the general protein import pore of mitochondria TOM-CC, this single molecule approach revealed a strong temporal correlation between lateral mobility and ion permeability, suggesting that the TOM-CC channel has mechanosensitive properties<sup>17</sup>. A lateral stop of freely moving TOM-CC molecules is accompanied by a partial or complete closure of the TOM-CC channel. Imaging DIB membranes with OmpF (**Figure 1E** and **Figure 4F**), which is almost fully embedded in the membrane, shows no stop-and-go effects (**Figure 5B**). Random stops of OmpF are not associated with a change in intensity and, thus, with the closing of its pores. Based on the fluorescence signals<sup>38</sup>, the positional accuracy of the individual channels can be estimated in the range between  $5$  and  $10 \text{nm}$ . However, it should be noted that this accuracy cannot be achieved if the channels wobble slightly due to mobile anchoring with the agarose hydrogel, as shown, for example, for the TOM-CC molecules in an intermediate state with a root mean displacement of  $120 \text{nm}$  (**Figure 5A**).

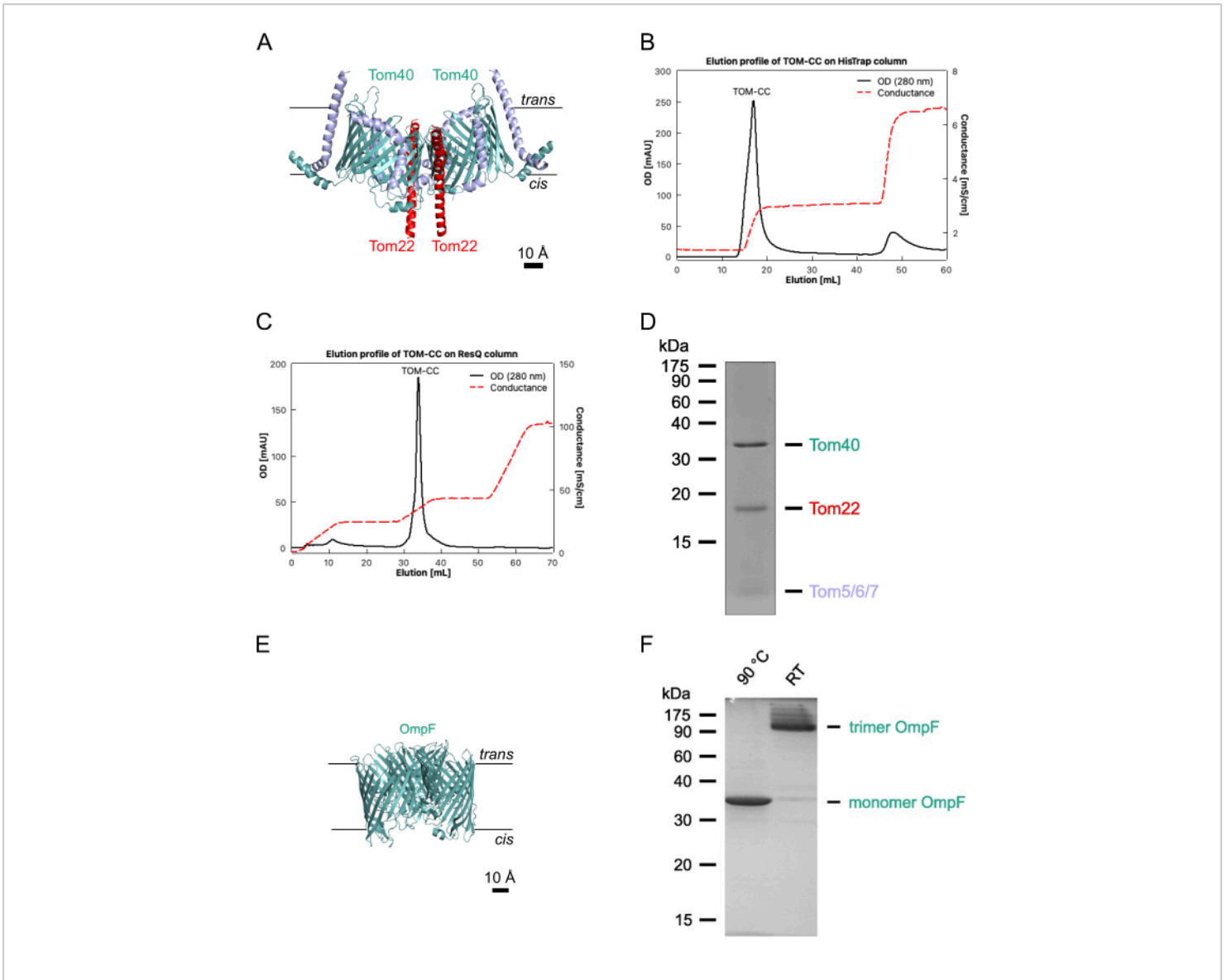


**Figure 1: Isolation of TOM-CC.** (A) Cryo EM structure of *N. crassa* TOM-CC<sup>30,39</sup>. Mitochondria from a *N. crassa* strain containing a Tom22 with a 6xHis tag were solubilized in DDM and subjected to Ni-NTA affinity chromatography (B) and anion-exchange chromatography (C). (D) SDS-PAGE of isolated TOM-CC. (E) Crystal structure (PDB, 1OPF) and (F) SDS-PAGE of purified *E. coli* OmpF. [Please click here to view a larger version of this figure.](#)

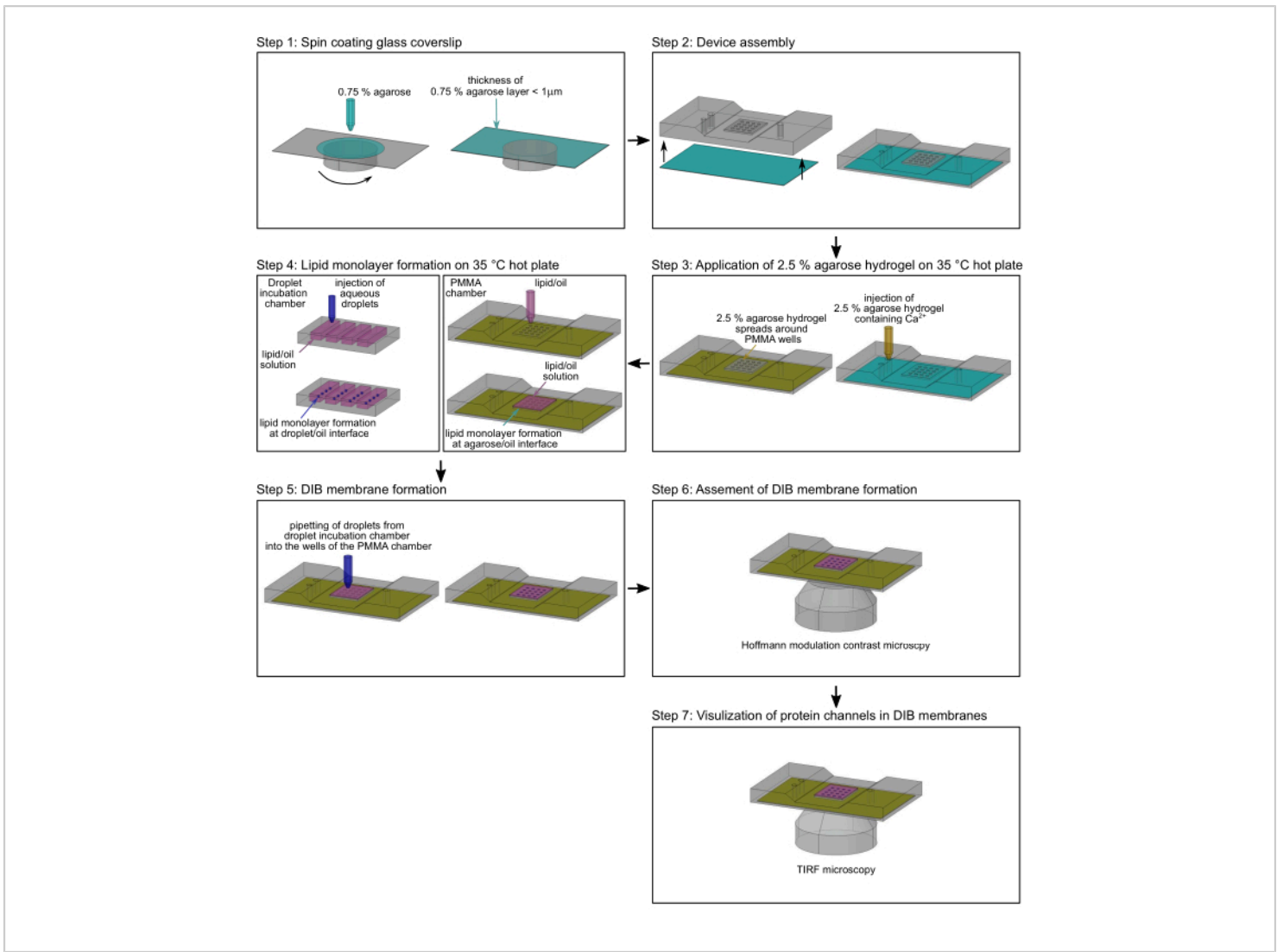


**Figure 2: Flow chart of PMMA chamber assembly.** Step 1: A glass coverslip is spin-coated with an agarose hydrogel. Step 2: The spin-coated coverslip is mounted in a custom-made PMMA microscopy chamber. Step 3: Additional low melt agarose is added into the inlet port of the PMMA chamber on a 35 °C hot plate. Step 4: Lipid monolayers are formed around aqueous droplets at a buffer/oil interface (left) and on the agarose hydrogel/oil interface (right). Step 5: Individual aqueous droplets are pipetted into the wells of the PMMA chamber to form a lipid bilayer upon contact of the two lipid monolayers. Step 6: Formation of the DIB membranes is validated by Hofmann modulation contrast microscopy. Step 7: Images of selected areas of the DIB membranes with inserted ion channels are acquired by TIRF microscopy. Green: 0.75% agarose; yellow: 2.5% agarose containing Ca<sup>2+</sup> ions; magenta: lipid/oil phase; dark blue: aqueous droplet buffer containing Ca<sup>2+</sup>-sensitive dye and protein. [Please click here to view a larger version of this figure.](#)

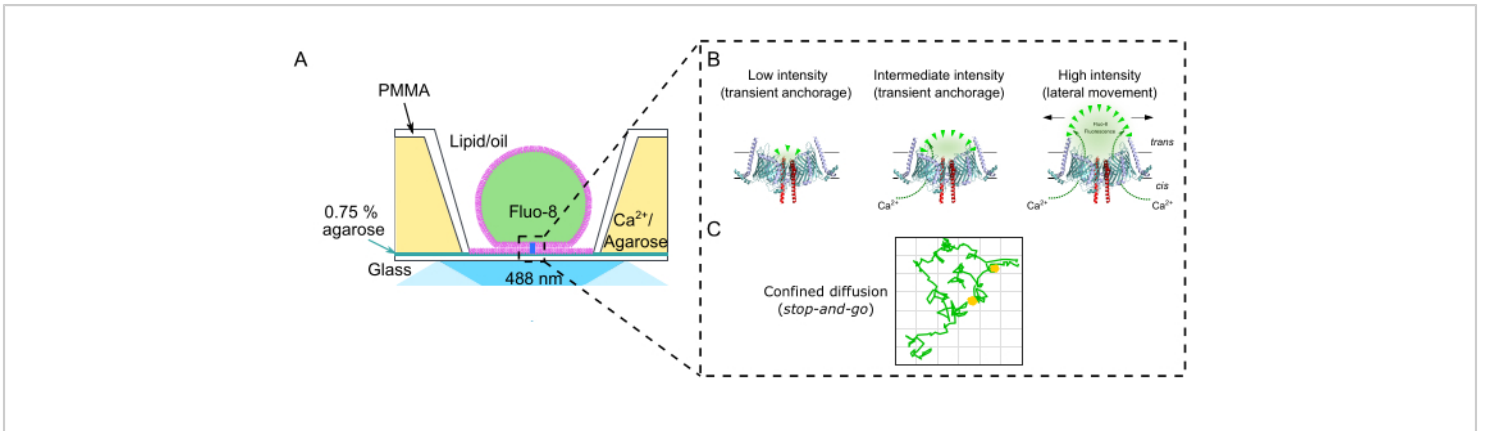


**Figure 3: Experimental setup.** (A) Schematic representation of a DIB membrane in a PMMA well. The bilayer rests on an ultrathin 0.75% agarose film to allow TIRF imaging of Ca<sup>2+</sup>-flux through an ion channel over time using a Ca<sup>2+</sup>-sensitive fluorescence dye (Fluo-8) in *trans*. (B) The Ca<sup>2+</sup>-flux is controlled exclusively by the osmotic pressure from *cis* to *trans*. This allows both the determination of the position in the membrane and the open-closed state of the channel. The channel shown here is the protein-conducting channel TOM-CC of *N. crassa* mitochondria<sup>30</sup>. (C) Trajectory of a single TOM-CC channel. Green: moving channel; yellow: non-moving channel. [Please click here to view a larger version of this figure.](#)

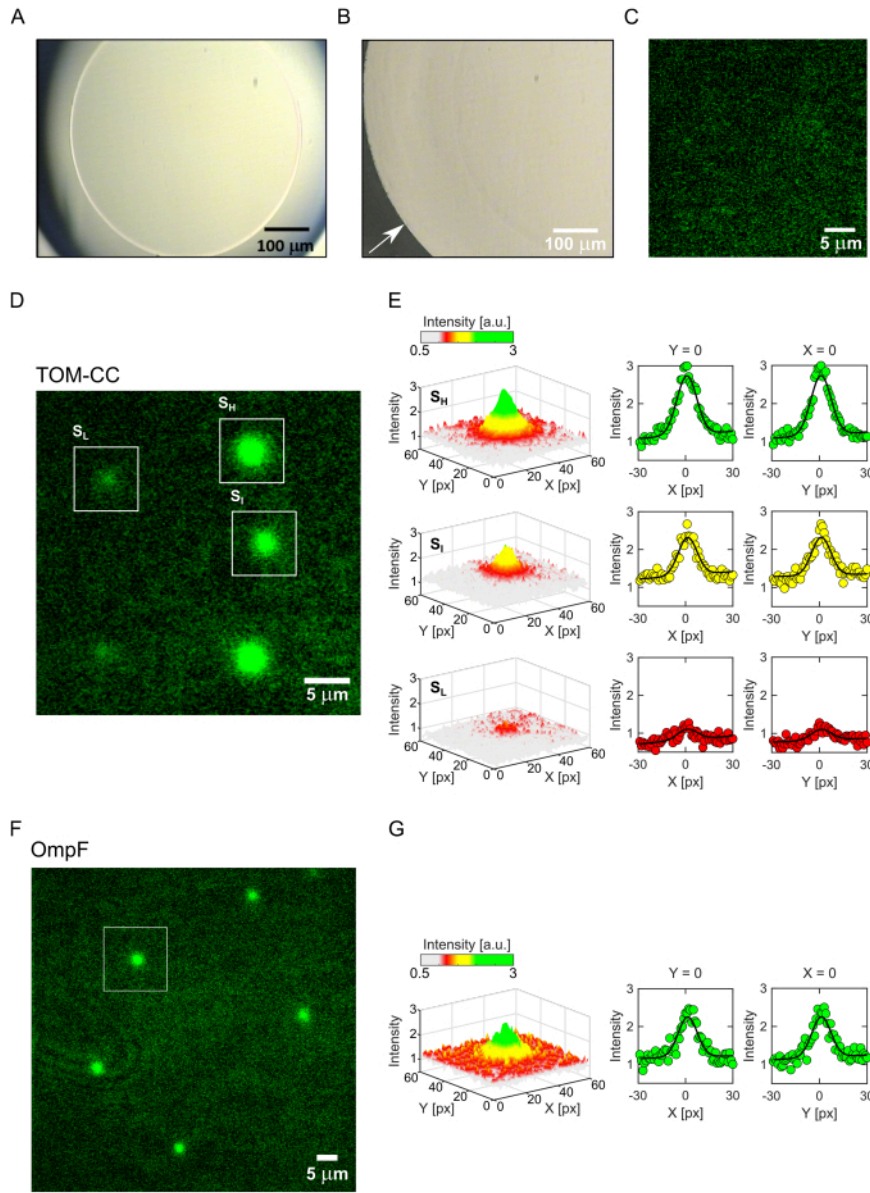


**Figure 4: Imaging TOM-CC and OmpF in DIB membranes.** (A) DIB membrane imaged by Hoffmann modulation contrast microscopy showing the bilayer contact area between the hydrogel and the droplet. (B) Broken DIB membrane imaged as in (A). Arrow, edge of PMMA chamber. (C) DIB membrane imaged by TIRF microscopy without protein channels. (D) DIB membrane with reconstituted TOM-CC, imaged by TIRF microscopy. The white squares mark spots of high (S<sub>H</sub>), intermediate (S<sub>I</sub>), and low (S<sub>L</sub>) intensity. (E) Fitting the fluorescence intensity profile of the three spots marked in (A) to two-dimensional Gaussian functions reveals the position of individual TOM-CCs and the Ca<sup>2+</sup> flux through the channel. (F) DIB membrane with reconstituted OmpF. (G) Gaussian fit of the fluorescent spot marked in (F). In contrast to the two-

pore  $\beta$ -barrel protein complex TOM-CC, the three-pore  $\beta$ -barrel OmpF reveals only one permeability state. Pixel size, 0.16  $\mu\text{m}$ . [Please click here to view a larger version of this figure.](#)

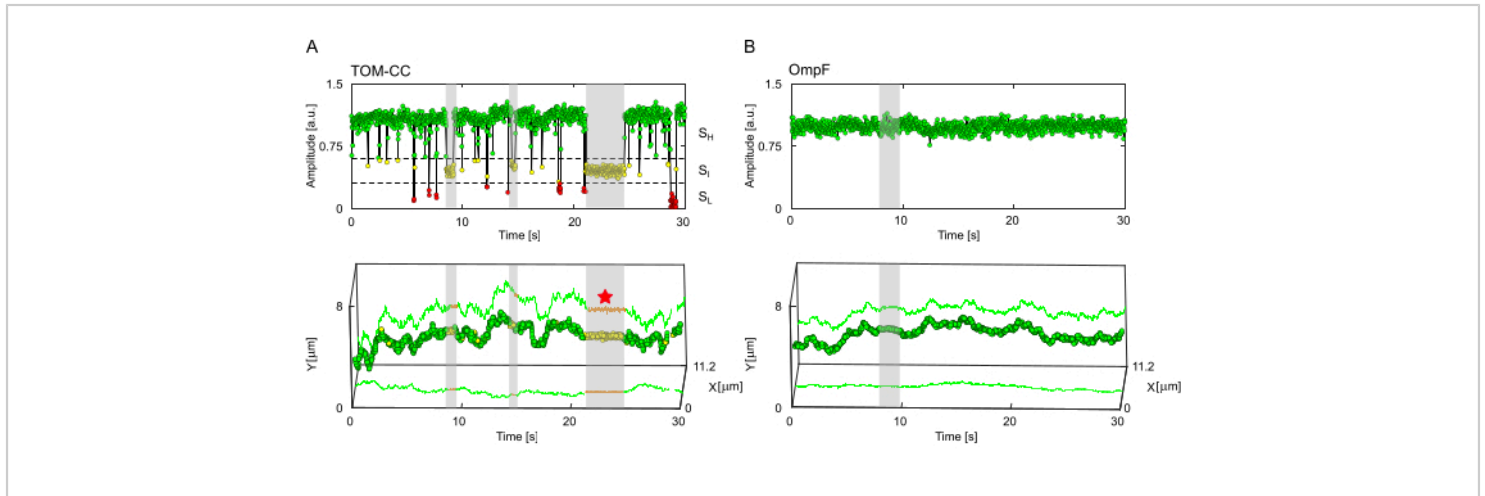


**Figure 5: Channel activity correlates with lateral mobility of TOM-CC.** (A) The fluorescent amplitude trace (top) and corresponding trajectory (bottom) of TOM-CC indicate that the open-closed channel activity of TOM-CC correlates with the lateral membrane mobility of the complex. The trajectory displays three permeability states. Green: fully open state; yellow: intermediate permeability state; red: closed channel state; red star: TOM-CC in the intermediate state wobbles around its mean position by about  $\pm 60$  nm. The positional accuracies<sup>37</sup> based on the fluorescence signals in the fully open and intermediate states range between 5 nm and 10 nm. (B) Fluorescent amplitude trace (top) and corresponding trajectory (bottom) of OmpF. OmpF reveals only one intensity level, regardless of whether it is in motion or trapped. The trajectory segments corresponding to the time periods of trapped molecules are marked in grey. [Please click here to view a larger version of this figure.](#)

Buffer	Reagent concentrations	Volume
A1*	20 mM Tris-HCl pH 8.5, 0.1 % (w/v) n-dodecyl- $\beta$ -D-maltoside (DDM), 10% (v/v) glycerol, 300 mM NaCl, and 1 mM phenylmethylsulfonyl fluoride (PMSF)	100 mL
A2*	20 mM Tris-HCl pH 8.5, 0.1% (w/v) DDM, 10% (v/v) glycerol, 1 M Imidazole and 1 mM PMSF	100 mL
B1*	20 mM HEPES pH 7.2, 0.1% (w/v) DDM, 2% (v/v) dimethyl sulfoxide (DMSO)	100 mL
B2*	20 mM HEPES pH 7.2, 0.1% (w/v) DDM, 1 M KCl, 2% (v/v) dimethyl sulfoxide (DMSO)	100 mL
* Degas and pass through a 0.22 $\mu$ m filter before use.		

**Table 1: Buffer solutions for TOM-CC isolation.**

Buffer	Reagent concentrations	Volume
LB*	1% (w/v) tryptone, 1% (w/v) NaCl and 0.5% (w/v) yeast extract	1100 mL
C1	2 mM MgCl <sub>2</sub> , and ~750 units DNase and 50 mM Tris-HCl pH 7.5	20 mL
C2	50 mM Tris-HCl, pH 7.5	50 mL
C3	4% (w/v) sodium dodecyl sulfate (SDS), 2 mM $\beta$ -mercaptoethanol and 50 mM Tris-HCl pH 7.5	50 mL
C4	2% (w/v) SDS, 500 mM NaCl and 50 mM Tris-HCl pH 7.5	50 mL
C5	0.5% (w/v) octyl polyoxyethylene (octyl POE), 1 mM EDTA and 20 mM Tris pH 8.5	1000 mL
* Sterilize before use.		

**Table 2: Buffer solutions for OmpF isolation.**

## Discussion

The protocol presented here provides an introduction to the use of DIB membranes to study the interplay between lateral ion channel movement and channel function using single-

molecule TIRF microscopy. To obtain the best possible data, the preparation of stable DIB membranes with as many well-separated channels as possible is crucial for obtaining

time series of individual particles, which can be analyzed satisfactorily.

Critical parameters to be optimized include the choice of lipid, the lipid concentration in the oil phase, and the protein and detergent concentrations in the aqueous droplets. The lipids employed are unusual, in that they show no clear phase transition at low temperatures. DPhPC is a commonly used lipid to produce stable membrane systems<sup>40</sup>. In principle, any lipid which maintains its fluid environment at low temperatures may be suitable for this application. In addition, the lipid should not be sensitive to oxidation. The detergent concentration in the droplets should be as low as possible to avoid membrane rupture. Stable membranes and good protein incorporation rates are generally achieved with detergent concentrations below the critical micelle concentration (cmc), given that the membrane protein does not precipitate.

If the DIB membranes do not tolerate specific detergents<sup>21,41</sup>, or if the proteins do not integrate from low detergent solution into the DIB membranes, the protein channels can first be reconstituted into small unilamellar lipid vesicles (SUVs), which are then fused to the DIB membranes from the droplet side, as has been successfully shown for *E. coli* MscL<sup>42</sup>. Sometimes, DIB membranes do not form because the lipid concentration in the oil phase is too low. To prevent DIB membranes from bursting, one should also be aware that the osmotic pressure between the hydrogel and the droplet must be precisely balanced without affecting the Ca<sup>2+</sup>-flux from *cis* to *trans* excessively. Optimized agarose thickness and mesh size seem to be crucial to observe the diffusion of membrane proteins. Any drying of the agarose layer should be avoided. The thickness can be determined using atomic force microscopy<sup>17</sup>. By

varying the agarose concentration, volume, and rotation speed during spin coating, the mesh size and thickness of the hydrogel can be optimized. Note, however, that hydrogel layer thickness affects image contrast. To capture membrane proteins in DIBs, the agarose hydrogel can be replaced by custom-synthesized, non-crosslinked, Ni-NTA-modified, low-melting agarose to trap them *via* a His-tag<sup>17</sup>. An excessively high fluorescence background is often caused by rupture of the DIB membranes. This is particularly a problem with multi-well chambers, as the Ca<sup>2+</sup>-sensitive dye diffuses into the hydrogel. In this case, adjacent wells should be avoided. Fluorescence bleaching of the Ca<sup>2+</sup>-sensitive dye above the membrane should not be a significant limiting factor, as it is exchanged by unexcited dyes in the bulk of the droplet (**Figure 3A**) outside the TIRF evanescent field. The localization precision for the protein is given by the accuracy of fitting the spots and the pixel size.

Weak fluorescence signals can be caused by low Ca<sup>2+</sup>-flux through the channel. Possible reasons include: (i) inaccurate TIRF settings (e.g., laser intensity), (ii) the osmotic Ca<sup>2+</sup> pressure across the membrane, or (iii) the intrinsic Ca<sup>2+</sup>-permeability of the channels is too low. To cope with the first issue, laser intensity, TIRF angle, and camera gain need to be optimized. The latter two issues can be overcome by the application of an electrical potential across the membrane<sup>2,43</sup>. However, the application of external voltages can distort the result, as electrical effects can influence the channel opening of ligand-gated or mechanosensitive ion channels that are actually not voltage-controlled. Examples of such channels are the mitochondrial protein translocase TOM-CC<sup>27</sup>, and its channel-forming subunit Tom40<sup>26,44,45,46</sup>. Finally, it should be noted that, inserting membrane proteins into DIB membranes in a specific orientation to achieve a desired functionality is tricky,

and quantitative studies are rare<sup>47,48</sup>. In some cases, the orientation of the integrated proteins is random. This is a serious problem for studying membrane proteins, because certain membrane proteins are activated on only one side of the membrane.

TIRF microscopy is a powerful method for addressing single-molecule events in planar supported membranes<sup>49</sup>. Examples include assembly and folding pathway elucidation of channel proteins such as  $\alpha$ -hemolysin<sup>50</sup>, perfringolysin O<sup>51</sup>, and OmpG<sup>52</sup>. These studies included FRET as an additional technique. In addition, activation of the mechanosensitive ion channel MscL has previously been studied by mechanical stimulation of supported DIB bilayers<sup>42</sup> using current measurements. Based on this work, future studies could combine the platform described here with single-molecule FRET experiments to address mechanosensitive channels at the single-molecule level in an optical manner<sup>17</sup>. Injection of buffer into the droplet, stretching the inner DIB monolayer, or targeted binding of individual channels to the underlying hydrogel can be used to further study not only the physical mechanism of mechanically activated channels, which respond to membrane tension and/or curvature as shown for MscL and MscS, the two-pore domain K<sup>+</sup>-channels, TREK-1, TREK-2, and TRAAK, and PIEZO (for review, see<sup>53</sup>), but also local binding to the cellular cytoskeleton, as shown for the touch-sensitive ion channel NOMPC<sup>54,55</sup>.

## Disclosures

We declare no conflicts of interest.

## Acknowledgments

We thank Beate Nitschke for her help with protein preparation and Robin Ghosh, Michael Schweikert (Stuttgart), and

Maximilian Ulbrich (Freiburg) for insightful discussions. This work was supported by the Stuttgart Research Center Systems Biology (SRCSB) and a grant from the Baden Württemberg Foundation (BiofMO-6 to SN).

## References

1. Tanaka, M., Sackmann, E. Polymer-supported membranes as models of the cell surface. *Nature*. **437** (7059), 656-663 (2005).
2. Leptihn, S. et al. Constructing droplet interface bilayers from the contact of aqueous droplets in oil. *Nature Protocols*. **8** (6), 1048-1057 (2013).
3. Thompson, J. R., Heron, A. J., Santoso, Y., Wallace, M. I. Enhanced stability and fluidity in droplet on hydrogel bilayers for measuring membrane protein diffusion. *Nano Letters*. **7** (12), 3875-3878 (2007).
4. Kusumi, A. et al. Paradigm shift of the plasma membrane concept from the two-dimensional continuum fluid to the partitioned fluid: high-speed single-molecule tracking of membrane molecules. *Annual Review of Biophysics and Biomolecular Structure*. **34** (1), 351-378 (2005).
5. Qian, H., Sheetz, M. P., Elson, E. L. Single particle tracking. Analysis of diffusion and flow in two-dimensional systems. *Biophysical Journal*. **60** (4), 910-921 (1991).
6. Kusumi, A., Shirai, Y. M., Koyama-Honda, I., Suzuki, K. G. N., Fujiwara, T. K. Hierarchical organization of the plasma membrane: Investigations by single-molecule tracking vs. fluorescence correlation spectroscopy. *FEBS Letters*. **584** (9), 1814-1823 (2010).
7. Betaneli, V., Schwille, P. Fluorescence correlation spectroscopy to examine protein-lipid interactions in

- membranes. *Methods in Molecular Biology*. **974**, 253-278 (2013).
8. Ando, T. et al. A high-speed atomic force microscope for studying biological macromolecules. *Proceedings of the National Academy of Sciences*. **98** (22), 12468-12472 (2001).
  9. Casuso, I. et al. Characterization of the motion of membrane proteins using high-speed atomic force microscopy. *Nature Nanotechnology*. **7** (8), 525-529 (2012).
  10. Karner, A. et al. Tuning membrane protein mobility by confinement into nanodomains. *Nature Nanotechnology*. **12** (3), 260-266 (2017).
  11. Rajendran, L., Simons, K. Lipid rafts and membrane dynamics. *Journal of Cell Science*. **118** (6), 1099-1102 (2005).
  12. Schink, K. O., Tan, K. -W., Stenmark, H. Phosphoinositides in control of membrane dynamics. *Annual Review of Cell and Developmental Biology*. **32** (1), 143-171 (2016).
  13. Schafer, D. A. Coupling actin dynamics and membrane dynamics during endocytosis. *Current Opinion in Cell Biology*. **14** (1), 76-81 (2002).
  14. Lingwood, D., Ries, J., Schwille, P., Simons, K. Plasma membranes are poised for activation of raft phase coalescence at physiological temperature. *Proceedings of the National Academy of Sciences*. **105** (29), 10005-10010 (2008).
  15. Engelman, D. M. Membranes are more mosaic than fluid. *Nature*. **438** (7068), 578-580 (2005).
  16. Jacobson, K., Liu, P., Lagerholm, B. C. The lateral organization and mobility of plasma membrane components. *Cell*. **177** (4), 806-819 (2019).
  17. Wang, S. et al. Spatiotemporal stop-and-go dynamics of the mitochondrial TOM core complex correlates with channel activity. *Communications Biology*. **5** (1), 471 (2022).
  18. Ide, T., Yanagida, T. An artificial lipid bilayer formed on an agarose-coated glass for simultaneous electrical and optical measurement of single ion channels. *Biochemical and Biophysical Research Communications*. **265** (2), 595-599 (1999).
  19. Funakoshi, K., Suzuki, H., Takeuchi, S. Lipid bilayer formation by contacting monolayers in a microfluidic device for membrane protein analysis. *Analytical Chemistry*. **78** (24), 8169-8174 (2006).
  20. Heron, A. J., Thompson, J. R., Mason, A. E., Wallace, M. I. Direct detection of membrane channels from gels using water-in-oil droplet bilayers. *Journal of the American Chemical Society*. **129** (51), 16042-16047 (2007).
  21. Bayley, H. et al. Droplet interface bilayers. *Molecular BioSystems*. **4** (12), 1191-1208 (2008).
  22. Huang, S., Romero-Ruiz, M., Castell, O. K., Bayley, H., Wallace, M. I. High-throughput optical sensing of nucleic acids in a nanopore array. *Nature Nanotechnology*. **10** (11), 986-991 (2015).
  23. Sackmann, E. Supported membranes: scientific and practical applications. *Science*. **271** (5245), 43-48 (1996).
  24. Kiessling, V., Yang, S. -T., Tamm, L. K. Supported lipid bilayers as models for studying membrane domains. *Current Topics in Membranes*. **75**, 1-23 (2015).

25. Murray, D. H., Tamm, L. K., Kiessling, V. Supported double membranes. *Journal of Structural Biology*. **168** (1), 183-189 (2009).
26. Hill, K. et al. Tom40 forms the hydrophilic channel of the mitochondrial import pore for preproteins. *Nature*. **395** (6701), 516-521 (1998).
27. Poynor, M., Eckert, R., Nussberger, S. Dynamics of the preprotein translocation channel of the outer membrane of mitochondria. *Biophysical Journal*. **95** (3), 1511-1522 (2008).
28. Künkele, K. P. et al. The preprotein translocation channel of the outer membrane of mitochondria. *Cell*. **93** (6), 1009-1019 (1998).
29. Ahting, U. et al. The TOM core complex: the general protein import pore of the outer membrane of mitochondria. *The Journal of Cell Biology*. **147** (5), 959-968 (1999).
30. Bausewein, T. et al. Cryo-EM structure of the TOM core complex from *Neurospora crassa*. *Cell*. **170** (4), 693-700.e7 (2017).
31. Cowan, S. W. et al. Crystal structures explain functional properties of two *E. coli* porins. *Nature*. **358** (6389), 727-733 (1992).
32. Bieligmeyer, M. et al. Reconstitution of the membrane protein OmpF into biomimetic block copolymer-phospholipid hybrid membranes. *Beilstein Journal of Nanotechnology*. **7**, 881-892 (2016).
33. Schindelin, J. et al. Fiji: an open-source platform for biological-image analysis. *Nature Methods*. **9** (7), 676-682 (2012).
34. Vicente, N. B., Zamboni, J. E. D., Adur, J. F., Paravani, E. V., Casco, V. H. Photobleaching correction in fluorescence microscopy images. In *Journal of Physics: Conference Series*. **90** (1), 012068 (2007).
35. Tinevez, J. -Y. et al. TrackMate: An open and extensible platform for single-particle tracking. *Methods*. **115**, 80-90 (2017).
36. Ershov, D. et al. TrackMate 7: integrating state-of-the-art segmentation algorithms into tracking pipelines. *Nature Methods*. **19** (7), 829-832 (2022).
37. Thompson, R. E., Larson, D. R., Webb, W. W. Precise nanometer localization analysis for individual fluorescent probes. *Biophysical Journal*. **82** (5), 2775-2783 (2002).
38. Hirsch, M., Wareham, R. J., Martin-Fernandez, M. L., Hobson, M. P., Rolfe, D. J. A stochastic model for electron multiplication charge-coupled devices - From theory to practice. *PLoS One*. **8** (1), e53671 (2013).
39. Bausewein, T., Naveed, H., Liang, J., Nussberger, S. The structure of the TOM core complex in the mitochondrial outer membrane. *Biological Chemistry*. **401** (6-7), 687-697 (2020).
40. Lindsey, H., Petersen, N. O., Chan, S. I. Physicochemical characterization of 1,2-diphytanoyl-sn-glycero-3-phosphocholine in model membrane systems. *Biochimica et Biophysica Acta*. **555** (1), 147-167 (1979).
41. Manafirad, A. Single ion-channel analysis in droplet interface bilayer. *Methods in Molecular Biology*. **2186**, 187-195 (2021).
42. Rosholm, K. R. et al. Activation of the mechanosensitive ion channel MscL by mechanical stimulation of supported Droplet-Hydrogel bilayers. *Scientific Reports*. **7** (1), 45180 (2017).

43. Wang, Y. et al. Electrode-free nanopore sensing by DiffusiOptoPhysiology. *Science Advances*. **5** (9), eaar3309 (2019).
44. Ahting, U. et al. Tom40, the pore-forming component of the protein-conducting TOM channel in the outer membrane of mitochondria. *The Journal of Cell Biology*. **153** (6), 1151-1160 (2001).
45. Romero-Ruiz, M., Mahendran, K. R., Eckert, R., Winterhalter, M., Nussberger, S. Interactions of mitochondrial presequence peptides with the mitochondrial outer membrane preprotein translocase TOM. *Biophysical Journal*. **99** (3), 774-781 (2010).
46. Kuszak, A. J. et al. Evidence of distinct channel conformations and substrate binding affinities for the mitochondrial outer membrane protein translocase pore Tom40. *The Journal of Biological Chemistry*. **290** (43), 26204-26217 (2015).
47. Yanagisawa, M., Iwamoto, M., Kato, A., Yoshikawa, K., Oiki, S. Oriented reconstitution of a membrane protein in a giant unilamellar vesicle: Experimental verification with the potassium channel KcsA. *Journal of the American Chemical Society*. **133** (30), 11774-11779 (2011).
48. Goers, R. et al. Optimized reconstitution of membrane proteins into synthetic membranes. *Communications Chemistry*. **1**, 35 (2018).
49. Castell, O. K., Dijkman, P. M., Wiseman, D. N., Goddard, A. D. Single molecule fluorescence for membrane proteins. *Methods*. **147**, 221-228 (2018).
50. Thompson, J. R., Cronin, B., Bayley, H., Wallace, M. I. Rapid assembly of a multimeric membrane protein pore. *Biophysical Journal*. **101** (11), 2679-2683 (2011).
51. Senior, M. J. T. et al. Single-molecule tracking of perfringolysin O assembly and membrane insertion uncoupling. *The FEBS Journal*. (2022).
52. Weatherill, E. E. et al. Fast slow folding of an outer membrane porin. *Proceedings of the National Academy of Sciences*. **119** (20), e2121487119 (2022).
53. Kefauver, J. M., Ward, A. B., Patapoutian, A. Discoveries in structure and physiology of mechanically activated ion channels. *Nature*. **587** (7835), 567-576 (2020).
54. Yan, Z. et al. Drosophila NOMPC is a mechanotransduction channel subunit for gentle-touch sensation. *Nature*. **493** (7431), 221-225 (2013).
55. Wang, Y. et al. The push-to-open mechanism of the tethered mechanosensitive ion channel NompC. *eLife*. **10**, e58388 (2021).